Journal of Medicinal Chemistry

Article

Deciphering the Role of Intramolecular Networking in Cholic Acid-Peptide Conjugates (CAPs) at Lipopolysaccharide Surface in Combating Gram-negative Bacterial Infections

Kavita Yadav, Sandeep Kumar, Deepakkumar Mishra, Mohammad Asad, Madhurima Mitra, Prabhu Srinivas Yavvari, Siddhi Gupta, Madhukar Vedantham, Pavit Ranga, Varsha Komalla, Sanjay Pal, Priyanka Sharma, Arti Kapil, Archana Singh, Nirpendra Singh, Aasheesh Srivastava, Lipi Thukral, and Avinash Bajaj

J. Med. Chem., **Just Accepted Manuscript** • DOI: 10.1021/acs.jmedchem.8b01357 • Publication Date (Web): 28 Jan 2019

Just Accepted

ACS Publications

is published by the American Chemical Society. 1155 Sixteenth Street N.W., Washington, DC 20036

Deciphering the Role of Intramolecular Networking in Cholic Acid-Peptide Conjugates (CAPs) at Lipopolysaccharide Surface in Combating Gram-negative Bacterial Infections

Kavita Yadav,[1,2,a] Sandeep Kumar,[1,2,a] Deepakkumar Mishra,[1] Mohammad Asad,[1] Madhurima Mitra,[1] Prabhu S. Yavvari,[3] Siddhi Gupta,[1] Madhukar Vedantham,[1] Pavit Ranga,[1] Varsha Komalla,[1] Sanjay Pal,[1,4] Priyanka Sharma,[5] Arti Kapil,[5] Archana Singh,[6] Nirpendra Singh,[7] Aasheesh Srivastava,[3] Lipi Thukral,[6,*] and Avinash Bajaj[1,*]

1. Laboratory of Nanotechnology and Chemical Biology, Regional Centre for Biotechnology, 3rd Milestone Faridabad-Gurgaon Expressway, NCR Biotech Science Cluster, Faridabad-121001, Haryana, India.
2. Manipal Academy of Higher Education, Manipal-576104, Karnataka, India.
3. Department of Chemistry, Indian Institute of Science Education and Research, Bhopal-462030, Madhya Pradesh, India.
4. Kalinga Institute of Industrial Technology, Bhubaneswar-751024, Odisha, India.
5. Department of Microbiology, All India Institute of Medical Sciences, Ansari Nagar, New Delhi-110029, India.
6. CSIR-Institute of Genomics and Integrative Biology, Mathura Road, New Delhi-110025, India.
7. Regional Centre for Biotechnology, 3rd Milestone Faridabad-Gurgaon Expressway, NCR Biotech Science Cluster, Faridabad-121001, Haryana, India.

a: authors contributed equally.

Corresponding Author:

Lipi Thukral, Email: lipi.thukral@igib.res.in

Avinash Bajaj, Email: bajaj@rcb.res.in

ABSTRACT

Presence of lipopolysaccharide and emergence of drug resistance make the treatment of Gram-negative bacterial infections highly challenging. Herein, we present the synthesis and antibacterial activities of Cholic Acid-Peptide conjugates (CAPs) demonstrating that Valine-Glycine dipeptide-derived CAP **3** is the most effective antimicrobial. MD simulations and structural analysis revealed that precise intramolecular network of CAP **3** is maintained in the form of evolving edges suggesting intramolecular connectivity. Further, we found high conformational rigidity in CAP **3** that confers maximum perturbations in bacterial membranes relative to other small molecules. Interestingly, CAP **3**-coated catheters did not allow the formation of biofilms in mice, and treatment of wound infections with CAP **3** was able to clear the bacterial infection. Our results demonstrate that molecular conformation and internal connectivity are critical parameters to describe antimicrobial nature of compounds, and analysis presented here may serve as a general principle for design of future antimicrobials.

INTRODUCTION

Microbial infections caused by Gram-negative bacteria pose a serious healthcare challenge due to emergence of multi-drug resistance towards existing antibiotics.[1] *Escherichia coli* (*E. coli*) is one of the major causative agent for skin and soft tissue infections especially in case of neonatal omphalitis, surgical site infections and infections after burn injuries.[2] *E. coli*-mediated nosocomial catheter-associated infections caused by drug resistant bacteria are a serious burden in medical settings.[3] Ability of the *E. coli* to form biofilms on skin or soft tissues and catheters make the treatment more difficult due to ability of biofilms to evade components of host immune response, stability of biofilms against mechanical forces, repeated infections and inability of the existing antibiotics to penetrate the enriched matrix of biofilms.[4,5]

Antimicrobials targeting key components of protein machinery may not adequately control the evolving drug-resistance as bacteria has the propensity to become resistant through accumulation of genetic mutations and evolutionary selection.[6] In contrast, bacterial membranes provide a suitable target for engineering of antimicrobial agents as targeting of membranes does not allow the bacteria to acquire drug resistance.[7] Membrane targeting of Gram-negative bacteria is more challenging over Gram-positive bacterial membranes due to presence of extra lipopolysaccharide (LPS) coated outer membranes[8] where lipid A-mediated bridge crosslinking creates a tough barrier for any toxic material.[9,10]

Lipopeptides (LPPs) and antimicrobial peptides (AMPs) are naturally occurring metabolites produced by host organisms as a part of innate immune system that can act against different pathogenic viral, bacterial and fungal infections.[11-12] Naturally isolated LPPs have a single hydrophobic chain attached to cyclic peptides making them amphiphilic in nature.[11] In contrast, α-helix and β-sheet-based natural AMPs provide required facial amphiphilic character with clear segregation of charge and hydrophobic amino acids.[12] Amphiphilic

nature of these LPPs and AMPs allow them to fold into certain structural conformations that is essential for executing antimicrobial activities. Therefore, numerous LPPs, AMPs and their derivatives have been engineered with different amino acid variations and hydrophobic tails,[13-16] but only few studies have stressed on the role of different structural conformations in antimicrobial activity.[17-20]

Cholic Acid (CA) scaffold, like AMPs, provides a facial amphiphilic character with three hydroxyl groups on its concave side.[21] Many CA-derived steroidal antimicrobials called Ceragenins have designed where CA was modified with charged amino groups along with different hydrophobic tails at carboxyl terminal.[22-24] However, the impact of natural amino acid-derived CA-peptide conjugates on antibacterial properties and their interactions with bacterial membranes at atomistic level has never been studied in detail.[25] Therefore, we undertook a systematic study to probe the antibacterial effect of all natural amino acid-derived peptides appended at CA scaffold against Gram-negative bacteria. In-depth molecular dynamics (MD) simulations followed by network analysis witnessed that tethering of Valine-Glycine dipeptides on CA (CAP **3**) provides required conformational rigidity for executing the effective interactions with bacterial membranes. Biophysical and biochemical assays validated that specific conformation stabilized by intramolecular interactions allows CAP **3** in executing membrane perturbations through specific contacts and in combating drug resistant, persistent, wound and catheter infections in *in vitro* and *in vivo* model systems.

RESULTS AND DISCUSSION

Design, synthesis and structure-activity relationship. We synthesized twenty CAPs with general chemical formula of CA-$(G\text{-}X)_3$ (referred as CA-X_3) where X is any natural amino acid conjugated to CA through a glycine linker (Figure 1A). For synthesis, CA (**21**) was first esterified with benzyl bromide in basic conditions to give benzyl cholate (**22**) in quantitative

yields (Figure S1). Boc protected glycines were then conjugated to three hydroxyl groups of benzyl cholate (**22**) using DCC/DMAP coupling followed by Boc deprotection using 4M HCl in dioxane. Different amino acids with suitable protecting groups were then attached to tri-glycine conjugated benzyl cholate (**23**) using diimide-based coupling reagents followed by deprotection as mentioned in Supplementary Information. All CAPs were characterized by ^{1}H NMR and HRMS and purity of CAPs (>95%) was confirmed by HPLC.

We then tested the antibacterial activity of CAPs against *E. coli* using broth dilution assay to determine the minimum inhibitory concentration at which 99% bacterial killing (MIC_{99}) was observed.[26] SAR studies revealed that basic and acidic amino acid-derived CAPs like **14** (CA-D_3), **15** (CA-E_3), **16** (CA-R_3), **18** (CA-K_3), **19** (CA-N_3) and **20** (CA-Q_3), and aromatic amino acid-derived CAPs like **8** (CA-F_3), **9** (CA-Y_3) and **10** (CA-W_3) are not active (Table S1). In contrast, CAPs appended with aliphatic amino acid residues like **1** (CA-G_3), **2** (CA-A_3), **3** (CA-V_3), **4** (CA-I_3), **5** (CA-L_3) and **7** (CA-M_3) are active in the range of 8-128 μM. Valine-derived CAP **3** (CA-V_3) and Isoleucine-derived CAP **4** (CA-I_3) are most active with MIC_{99} of 8 μM (Table S1). SAR against other Gram-negative bacteria *Klebsiella pneumoniae* and *Acinetobacter baumannii* witnessed that CAP **3** and CAP **4** are active at 16 μM (Table S1). Hemolytic activity of CAPs against human red blood cells (RBCs) and cytotoxicity against epithelial cells (A549) revealed that CAP **4** is highly toxic towards RBCs and epithelial cells without any selectivity for bacterial membranes (Table S1). In contrast, CAP **3** was ~6-7 fold selective for *E. coli* over RBCs and epithelial cells. To overrule the detergent-mediated effect of CAP **3**, we studied the self-assembled properties of CAP **3** and determined the critical miceller concentration (CMC) of CAP **3**. CAP **3** did not show any aggregation up to 100 μM (CMC > 100 μM) confirming the non-detergent-mediated antibacterial effect of amphiphile.

Natural AMPs and LPPs are usually rich in basic amino acids like lysine, arginine or polar hydrophobic amino acids like tryptophan that allows them to bind effectively with bacterial membranes.[27] In contrast, above results witnessed that lysine, arginine and tryptophan-derived CAPs did not show any antibacterial activity. To understand this SAR, we selected most active hydrophobic valine-derived CAP **3** and three inactive CAPs based on polar hydrophobic tryptophan (CAP **10**), acidic glutamic acid (CAP **15**) and basic lysine (CAP **18**) amino acids (Figure 1B). We compared their interactions with LPS-derived membranes using computational, biophysical and biochemical approaches.

Biomolecular simulations. We performed all-atom molecular dynamics simulations to study the differential binding modes of the selected CAPs with model Gram-negative bacterial membranes.[28] Four independent molecular systems containing complex LPS of Gram-negative bacteria were generated that mimic the experimentally tested molecular process. Gram-negative outer membrane model consists of LPS molecules in the outer leaflet and varied phospholipids in inner leaflet to simulate the physiologically relevant bacterial membrane interface (Figure S2, Table S2).[29,30] The starting structure representation was prepared with no prior membrane contacts (Figure S3A), and after 300 ns, subtle changes in membrane architecture were observed (Figure S3B). Towards the end of the simulation at 500 ns, CAPs displayed varied membrane permeabilization activity. In particular, CAP **3** was completely inserted within the outer leaflet comprising of LPS molecules (Figure 2A). CAP **15** also showed partial insertion, whereas CAP **10** and CAP **18** could execute relatively few membrane interactions (Figure 2A). The contour maps shown in Figure 2B depict top view of the simulation box after 500 ns with each grid value showing membrane thickness that represents the distance between upper and lower membrane atoms. Significant membrane thinning in CAP **3**-membrane complex was observed with scattered blue color patches of ~2 nm thickness representing compressed

membranous structures. CAP **10** and **18** did not cause any thinning of membranes, whereas we observed CAP **15** induced membrane thinning to some extent (Figure 2B).

Above results revealed a clear trend, where CAP **3** causes maximum disruptions to the membrane architecture and CAP **18** showed poor interactions with membranes in spite of being appended to basic charged amino acids. As molecular crowding is a key factor in antimicrobial activity, we ran additional simulations with higher concentrations of CAP **3** where two independent structures were generated containing membranes with 5 and 20 molecules of CAP **3** in water environment (Figure S4). As a consequence, severe membrane defects were observed as compared to control (only membrane) trajectories (Figure S4). These findings demonstrate the ability of CAP **3** to integrate into the bacterial LPS groups and cause significant structural variations.

We then characterised four segments of bacterial membranes, O-Antigen, outer and Inner polysaccharides, lipid A and phospholipids to depict the precise binding site differences of CAPs with bacterial membranes. We found that CAP **3**, most active antibacterial, favourably interacts with inner polysaccharides of bacterial membranes (Figure S5A). In contrast, inactive CAPs **10**, **15** and **18** reside on the surface of bacterial membranes and interact with the outer core polysaccharides (Figure S5B-D). Remarkably, the core fold of CAP **3** was inserted completely to interact with O-antigen segment through polar interactions (Figure S5A). In contrast, position of other CAPs were not able to form an inward or membrane facing binding pocket and therefore could not perform same interactions as that of CAP **3** (Figure S5B-D).

To understand the toxicity differences observed between CAP **3** (less toxic) and CAP **4** (more toxic) against mammalian cells, we also performed simulations of these molecules (CAP **3** and CAP **4**) with model mammalian cell membranes (Table S2). The atomistic trajectories of these two molecules with DPPC-cholesterol molecules (model membranes)

were generated to mimic the mammalian membranes. CAP **4** showed immediate membrane penetration as compared to CAP **3** that was residing only at the surface of membrane without any insertion (Figure S6A-B). The kinetic calculations of the distance showed increased membrane contacts of CAP **4** as compared to CAP **3** (Figure S6C). Number of contacts in case of CAP **4** significantly increased from 40 to ~80 as compared to CAP **3** that did not show any significant increase in number of contacts (Figure S6D). Therefore, favorable interactions of CAP **4** with mammalian cell membranes make it more toxic than CAP **3**.

Savage's group has performed fluorescence-based studies to decipher the interactions of CA-derived amphiphiles (Ceragenins) with Gram-negative membranes, and proposed that lipid A component of LPS is responsible for interactions of these antimicrobials with bacterial membranes.[22,23] They also synthesized water soluble derivative of Lipid A and fluorophore-derivatives of cationic steroids and compared the binding abilities of Ceragenins with lipid A.[22,23] In contrast, our studies provided atomistic level interactions of CA-derived amphiphiles with bacterial membranes.

Structural analysis of CAPs. We then undertook a detailed survey of molecular conformations adopted by these CAPs. Values of root mean square fluctuations (RMSF) were calculated and mapped onto chemical structures as shown in Figure 3A. CAP **10** was the most flexible with highest RMSF of 0.73 nm (Figure 3A, S7A). Interestingly, CAP **3** showed rigid conformational character with lowest RMSF value of 0.42 nm. These values were then decomposed depending on the atoms of cholic acid and side-chain where cholic acid atoms, a common denominator across all molecules, showed considerable changes in all CAPs except for CAP **3** (Figure S7B). In contrast, side-chain atoms for all CAPs were highly mobile and dynamic during interactions with membrane groups (Figure S7C).

To determine the most commonly occurring conformations, we performed clustering on all structures within each trajectory and selected top clusters (Figure S8). Top clusters for CAPs

10 and **15** trajectories showed only ~11.8 and ~22.4% due to varying number of conformations in these CAPs (Figure S8). CAP **3** exhibited similar conformation as the top cluster was present in ~94.56% probability whereas CAP **18** existed in a conformation with 90% probability. Superimpositions of all the top clusters revealed structural variability in each CAP that clearly witnessed the rigidity of CAP **3** over other CAPs (Figure 3B). Therefore, structural analysis of CAPs confirmed that chemical space of CAP **3** is highly rigid and this unique interfacial conformational state may be directly coupled to its potent activity towards membrane permeabilization.

Intra-molecular network-based analysis. We then quantified the number of membrane contacts and hydrogen bonds formed by each CAP with membrane surface, and observed that both membrane contacts and hydrogen bonds increased as a function of time for all the CAPs (Figure S9). CAPs **3** and **15** formed minimal membrane contacts (Figure S9A). Kinetic plots demonstrated the ability of these molecules to form strong interactions with membranes where CAP **3** is perturbing the membranes with relatively few non-covalent interactions (Figure S9B).

In order to probe the differential interactions executed by these CAPs, we studied the dynamics of intra-molecular interactions in CAPs at LPS membrane surface. We utilized the network approach analogous to Residue Interaction Network (RIN) that is computed widely for intra-protein interactions.[31-32] In this network analysis, interactions among different atoms within a molecule correspond to “edges” and number of atoms within molecule correspond to “nodes”. Specifically, the nodes stay constant and edges are dynamically formed by non-covalent interactions during the length of the simulations. In order to probe geometric arrangements between nodes and edges, we computed networks for CAPs at 0 and 500 ns. Global network topology derived from structures of CAPs shown in Figure S10-S13 suggests that networks are dense with disparate nodes towards the periphery. We then computed

general network parameters about centrality and connectedness of the networks and witnessed that several edges are contributed from CA backbone atoms (Figure 4).

Further, we quantified the dynamic parameters of networks and noticed that CA backbone presented “hub” features across all the CAPs. The hubs are defined as nodes that have stable and more number of interactions. Comparison of all nodes (in particular 20-64 nodes) representing CA backbone atoms (or hub) of CAPs suggested that only CAP **3** execute new interactions within molecule after 500 ns with 885 edges whereas only 868 interactions were observed at 0 ns (Figure 4, Figure S14). In contrast, significantly lesser number of edges are formed in other three CAPs (Figure 4, Table S3). In addition, side-chain atoms of CAP **3** also contributed to this increase where benzene ring interacts heavily with the backbone atoms (Figure S10). We observed that interactions between side-chain atoms and CA backbone in other CAPs are highly dynamic (Figure S11-S13, Figure S14).

Our network analysis therefore suggests that transition from starting conformational state to other structures occurs through dynamic changes within CAP **3**. In particular, new edges (interactions) are formed within the molecule in different parts of chemical space. These findings suggested that intra-molecular interactions compensated with low membrane contacts formed by CAP **3** may directly aid in membrane perturbation behavior. To test how the order parameters calculated from MD simulations can rank the molecules based on activity, we ran additional simulations of CAP **4** (antibacterial like CAP **3**) and CAP **9** (inactive against bacteria) with model bacterial membranes. CAP **4** showed full insertion into the bacterial membranes (Figure S15A-B) as compared to interfacial contacts made by CAP **9** (Figure S15C-D). Quantification of membrane thickness witnessed CAP **4**-mediated enhanced thinning of bacterial membranes as compared to CAP **9** (Figure S15E) and RMSF calculations confirmed more rigidity of CAP **4** over CAP **9** amphiphile (Figure S15F). Time calculations of membrane contacts and hydrogen bonding could not capture any molecular

differences (Figure S16A, S16B). In contrast, intramolecular networking of CAP **4** revealed higher number of edges with increased intramolecular networking as compared to CAP **9** on interactions with bacterial membranes (Figure 16C-D). Therefore, these simulations validate that intramolecular networking of small molecules may accurately predict the activity of small molecules with high precision.

Validation of CAP-LPS Interactions. We then validated the differential interactions of the selected CAPs with model membranes as depicted by MD simulations using biophysical and biochemical assays. To assess the impact of CAPs on membrane rigidity, we first prepared diphenylhexatriene (DPH)-doped model Gram-negative bacterial vesicles using LPS, DPPE and DMPG lipids,[33] and measured the change in DPH anisotropy on incubation with CAPs. We observed ~2-fold increase in fluidity of membranes on incubation with CAP **3** whereas insignificant change in rigidity was observed on incubation of other CAPs (Figure 5A). We then evaluated the comparative binding affinities of these CAPs with LPS using Dansyl-Polymyxin B displacement assay where complexes of LPS with Dansyl-labelled Polymyxin B were titrated with CAPs and change in fluorescence was quantified (**10** was insoluble in water and not tested further).[34] Increase in fluorescence of Dansyl-Polymyxin B due to its displacement from LPS complexes confirmed the strongest affinity of CAP **3** for LPS over other CAPs (Figure 5B). Similarly, increase in fluorescence on titrations of CAPs with fluorescent boron-dipyromethane conjugated LPS (BODIPY-LPS) established that CAP **3** can bind and disintegrate the LPS aggregates more effectively than other CAPs (Figure 5C).[35]

We then assessed the relative membrane binding affinities of CAPs using Surface Plasmon Resonance (SPR)[36] where CAP **3** showed highest binding response with irreversible binding among all the CAPs (Figure 5D-5F). Analysis of overall affinity constant (K_A) witnessed highest binding of CAP **3** over CAP **15** and CAP **18**.[37] Comparison of K_1 and K_2 revealed

that second step involving integration of antimicrobials into bacterial membranes is responsible for higher K_A for CAP **3** (Figure 5G). This strong association of CAP **3** in second step might be due to presence of balanced charge and hydrophobicity in valine-derived CAP **3** that allows electrostatic interactions followed by hydrophobic integration in bacterial membranes.

Bactericidal effect of CAP 3. To further validate the differential interactions of CAPs with bacterial membranes, we compared the abilities of CAPs to permeabilize the outer bacterial membranes in *E. coli* using *N*-phenyl naphthylamine (NPN) fluorescent dye as its fluorescence gets enhanced on penetration in disrupted hydrophobic membranes.[38] Comparison of permeation assay witnessed that CAP **3** is more effective in permeabilization of outer bacterial membranes over other CAPs (Figure 6A). Interactions of membrane targeting antimicrobials in general induce depolarization of the membranes and release of accumulated quenched fluorescent dyes like 3',3'-diethylthiadicarbocyanine $DiSC_2(5)$ from depolarized membranes results in enhanced fluorescence.[39] Comparative analysis of CAPs confirmed CAP **3**-mediated increase in fluorescence of $DiSC_2(5)$ thereby making it most effective in depolarization of bacterial membranes (Figure 6B). Quantification of the uptake of membrane impermeable dye propidium iodide (PI) by bacteria on treatment with different CAPs revealed CAP **3**-induced significant increase in number of PI positive cells (Figure 6C). Microscopy studies showed the uptake the PI confirming the membrane lytic nature of the CAP **3** (Figure S17A). To confirm the LPS-mediated interactions of CAP **3** with bacterial membranes, we tested the antibacterial activity of CAP **3** against *E. coli* in presence of LPS and measured the percentage of PI positive cells. We observed LPS-mediated dose dependent inhibition of PI uptake by *E. coli* on CAP **3** treatment thereby confirming the effective CAP **3**-LPS interactions (Figure S17B). Therefore, above studies validated the SAR and our observations from MD simulations where valine-derived CAP **3** was found most

effective in binding with LPS membranes over other CAPs that is responsible for its antibacterial effect.

We then performed time dependent killing assay where bacteria (*E. coli*) were treated with CAP **3** for different time and CFUs were quantified. We did not observe any colony after 6h of CAP **3** treatment at 1X MIC_{99} and 90 min of CAP **3** treatment at 4X MIC_{99} was sufficient to kill most of the bacteria (Figure 6D). Impact of CAP **3** on membrane morphology was then assessed using transmission electron microscopy where untreated bacteria showed a smooth rod-shaped morphology and CAP **3** treatment induced distinct morphological changes with distorted shapes and 'kinks' in the bacterial membrane (Figure 6E).

Major challenge for use of any antimicrobial is the ability of bacteria to develop resistance against antimicrobials.[40] Therefore, we tested the ability of *E. coli* to develop resistance against CAP **3** and observed that *E. coli* was unable to develop resistance against the CAP **3** whereas there was multi-fold increase in MIC_{99} of neomycin (Figure 6F). Antimicrobial activity of CAP **3** against stationary and persistent *E. coli* cells established that CAP **3** was able to kill the stationary and persistent bacteria where ampicillin was ineffective (Figure 6G). Antibacterial activities at different CFUs of *E. coli* validated that CAP **3** was also able to clear the bacterial growth even at CFUs of 10^{12}/mL, making it highly potent antimicrobial (Figure 6H).

Activity against biofilms. Biofilms usually respond poorly to antibiotic therapy and are responsible for inducing antibiotic resistance due to increased mutation rates, high expression of efflux pumps and trapping of antibiotics in exopolysaccharide matrix.[41] Therefore, we assessed the ability of CAP **3** to disrupt the *E. coli* biofilms. Pre-formed *E. coli* biofilms were treated with different concentrations of CAP **3** for 24h and were quantified by CFU analysis. A dose dependent decrease in CFUs was observed on CAP **3** treatment and CAP **3** at 64 μM (8X MIC_{99}) resulted in a ~8-log fold decrease in CFU (Figure 7A). Crystal

violet staining witnessed ~90% decrease in biofilm mass after treatment with CAP **3** at 8X MIC_{99} (Figure 7B). Although the concentrations for biofilm degradation are much higher than the toxic concentration of the amphiphile for mammalian cells, it should be noted that the experimental biofilms used here are very thick in nature with high bacterial load that is not usually observed in clinical settings. Bactericidal nature of CAP **3** on biofilms was then established using SYTO9-PI staining where SYTO9 can permeabilize and stain all the bacteria and PI can only permeabilize and stain dead bacteria. Confocal laser scanning micrographs (CLSM) of untreated biofilms stained with SYTO9-PI showed thick biofilm mass of viable SYTO9-stained green fluorescent *E. coli* bacteria without any visible PI-stained red bacteria (Figure 7C, upper panel). CAP **3** treatment resulted in increase of PI-stained *E. coli* establishing the bactericidal and biofilm disrupting effect of CAP **3** (Figure 7C, lower panel). Quantification of the biofilm thickness confirmed significant reduction in biofilm formation on CAP **3** treatment (~ 3 μm) as compared to untreated biofilms (>8 μm) (Figure 7D). Scanning electron microscopy (SEM) was then performed to understand the effect of CAP **3** on architecture of *E. coli* biofilms. Untreated biofilms presented a thick biomass with rod shape (*E. coli*) bacteria forming an extensive network of pores and channels that helps in distribution of nutrients (Figure 7E). CAP **3** treatment unsettles this network and breakdowns the extracellular architecture by disrupting the bacterial membranes and by creating isolated lytic bacteria (Figure 7E).[42] Therefore, these results establish the ability of the CAP **3** to interact with Gram-negative bacteria submerged in thick biofilms and clear them.

***In vivo* activity.** As *E. coli*-mediated catheter and wound infections are very common, we first tested the ability CAP **3**-coated catheters to prevent the biofilm formation during *in vitro* conditions. Sterilized catheter pieces (~1 cm) were first coated with CAP **3** where catheters were dipped in solution of CAP **3** in dichloromethane (DCM) and DCM was evaporated

providing CAP **3**-coated catheters. These coated catheters were dipped in *E. coli* suspension for three days and CFU analysis confirmed the absence of any adhered bacteria on CAP **3**-coated catheters whereas significant amount of bacterial coating was observed on uncoated and control (DCM)-coated catheters (Figure 8A). To test the efficacy of CAP **3**-coated catheters in preventing biofilm formation in mice, uncoated, DCM (control)- and CAP **3**-coated catheter pieces (~1cm, 1 catheter/mice, 4 mice/group) were inserted subcutaneously in an incision on the flank of mice[43] and these incised sites were infected with *E. coli*. CFU analysis confirmed that there was no adherence of any bacteria on CAP **3**-coated catheters after three days unlike uncoated and control catheters establishing the ability of CAP **3** in preventing bacterial growth in murine models (Figure 8B).

To assess the efficacy of CAP **3** in clearing the wound infections,[44] we first created the wounds on BALB/c mice and infected them with *E. coli* strain. After 6h of infection, mice were randomized into four groups (3 mice/group) and were either left untreated (group 1) or treated with ampicillin (40mg/kg) (group 2) or CAP **3** (40mg/kg) (group 3) or neomycin (40mg/kg) (group 4) thrice daily for four days. CFU analysis on day 5 witnessed significant reduction in bacterial load on wound where ampicillin was less effective (Figure 8C). We then performed bioluminescence imaging of mice infected with *E. coli* bioluminescent strain (Xen14) and observed significant decrease in bioluminescence on CAP **3** treatment confirming its bactericidal effect (Figure 8D). These results therefore establish that CAP **3** can act as bactericidal in clearing wound infections.

To validate the therapeutic efficacy of CAP **3** against multi-drug resistant strains, antibacterial activity of CAP **3** was tested against different multidrug-resistant clinical strains of *E. coli*, *A. baumannii* and *K. pneumoniae*. CAP **3** was active in range of 4-16 μM (MIC_{99}) against all clinical strains and activity was in range of 4-8 μM (MIC_{99}) for *E. coli* strains (Figure 8E).

CONCLUSIONS

In this work, we presented the design of CA-peptide conjugates to decipher the impact of all-natural amino acids on antibacterial activities against Gram-negative bacterial species. Twenty CAPs were engineered where different natural amino acids were appended on hydroxyl groups of benzylated cholic acid using a glycine linker. SAR witnessed that basic charged amino acid like lysine, arginine and histidine, and polar hydrophobic amino acid likes tryptophan and proline-derived CAPs are inactive in spite of their charged nature, whereas valine-derived CAP **3** is the most active. Comparative MD simulations with LPS model membranes revealed atomistic features with CAP **3**, mediating maximum thinning of bacterial membranes over other CAPs. Structural and network analysis witnessed stable conformation of CAP **3** and enhanced intramolecular networking that allowed it to perform specific interactions with bacterial membranes. Mechanistic studies confirmed LPS-mediated bactericidal nature of CAP **3** that allowed it to kill drug resistant bacteria and degrade/prevent the biofilms in murine models. Therefore, this report provides a mechanistic understanding of membrane perturbations in context of detailed structural and molecular information of CAPs and explain how intramolecular network of a given antimicrobial is the distinguishing factor.

EXPERIMENTAL SECTION

1. Synthesis of CA-peptide (CAPs) conjugates. Detailed synthesis, characterization and spectral data of all the molecules is described in Supporting information. Purity of the compounds was tested by HPLC and found to be more than 95%.

2. Other experimental details. Computational methods used, microorganisms and culture conditions, antibacterial assay, hemolytic assay, cytotoxicity assay, biophysical assay for studying amphiphile model membrane interactions, membrane permeabilization studies, activities against biofilms, *In vitro* catheter assay, *in vivo* catheter infection studies, *in vivo*

bioluminescence imaging and activity assay against clinical strains are detailed in supporting information.

3. Ethics statement. All animal experiments were performed after due ethical approval from Institutional Animal Ethics Committee of Regional Centre for Biotechnology (RCB/IAEC/2016/001). All experiments with human blood samples and clinical bacterial isolates were performed after due ethical approval from Institute Ethics Committee of All India Institute of Medical Sciences (IEC/NP-433/09/10.2015) and Regional Centre for Biotechnology (RCB-IEC-H-7).

SUPPORTING INFORMATION

Supporting figures S1-S17, supporting tables S1-S4, molecular formula strings, materials and methods, detailed synthesis of molecules and other experimental details like computational methods used, microorganisms and culture conditions, antibacterial assay, hemolytic assay, cytotoxicity assay, biophysical assay for studying amphiphile model membrane interactions, membrane permeabilization studies, activities against biofilms, *in vitro* catheter assay, *in vivo* catheter infection studies, *in vivo* bioluminescence imaging and activity assay against clinical strains are available in supporting information.

AUTHOR CONTRIBUTIONS

K.Y. performed bacterial culture and cell culture-based studies. D.M., P.R., V.K. and S.K. synthesized and characterized all the CAPs. K.Y., P.S.Y., S.P. and M.V. performed animal experiments. M.A. performed computational studies. M.M. performed SPR and other biophysical experiments. S.G., M.V. and P.S.Y. performed in vitro biofilm experiments. S.G. and A.S. processed samples for TEM studies. P.S. and A.K. helped in screening of clinical strains. P.S.Y. performed SEM experiments and A.S. supervised it. L.T. supervised the computational studies. A.B. conceived the idea, designed the experiments and supervised

the whole project. Manuscript was written by K.Y., S.K., L.T. and A.B. and approved by all the authors.

ACKNOWLEDGEMENTS

We are grateful to RCB, IGIB, IISER and AIIMS for intramural funding. Work in A.B. laboratory is supported by the following grants: BT/PR12297/MED/29/895/2014 (DBT) and BT/PR17525/MED/29/1021/2016 (DBT). P.S.Y and S.P. thank UGC, and K.Y. and S.K. thank RCB for research fellowships. Financial support from the DBT-RA Program in Biotechnology and Life Sciences is gratefully acknowledged. Small animal facility of Regional Centre for Biotechnology is supported BT/PR5480/INF/22/158/2012 (DBT). A.S. is supported by BT/PR17525/MED/29/1021/2016 (DBT). L.T. thanks support from CSIR intramural funding for this project under MLP 1805 grant. We thank CSIR-4PI for supercomputing resources, and TEM facility at CSIR-IGIB. We also thank the support of DBT e-Library Consortium (DeLCON) for providing access to e-resources.

AUTHOR INFORMATION

***Corresponding Author: Email: bajaj@rcb.res.in;** Tel: 0091-129-2848831.

ORCID

Avinash Bajaj: 0000-0002-1333-9316

Notes: Authors declare no competing financial interests.

ABBREVIATIONS USED

CA, Cholic Acid; LPPs, lipopeptides; AMPs, antimicrobial peptides; CAP, cholic acid-peptide conjugate; CMC, Critical miceller concentration; DPPC, Dipalmitoylphosphatidylcholine; RMSF, root mean square fluctuations, DPH, diphenylhextatriene, DPPE, 1,2-Dipalmitoyl-sn-glycero-3-phosphoethanolamine DMPG, 1,2-Dimyristoyl-sn-glycero-3-phosphorylglycerol sodium salt; NPN, N-phenyl naphthylamine, $DiSC_2(5)$, 3',3'-diethylthiadicarbocyanine; PI, Propidium Iodide, CFUs, colony forming units.

REFERENCES

1. Kaper, J. B.; Nataro, J. P.; Mobley, H. L. T. Pathogenic *Escherichia coli*, *Nat. Rev. Microbiol.* **2004**, *2*, 123-140.

2. Petkovšek, Ž.; Eleršič, K.; Gubina, M.; Žgur-Bertok, D.; Erjavec, M. S. Virulence Potential of Escherichia coli Isolates from Skin and Soft Tissue Infections. *J. Clin. Microbiol.* **2009,** *47*, 1811-1817.

3. Jacobsen, S. M.; Stickler, D. J.; Mobley, H. L. T.; Shirtliff, M. E. Complicated Catheter-Associated Urinary Tract Infections Due to *Escherichia coli* and *Proteus mirabilis*. *Clin. Microbiol. Rev.* **2009**, *21*, 26-59.

4. Bjarnsholt, T.; Alhede, M.; Alhede, M.; Eickhardt-Sørensen, S. R.; Moser, C.; Kühl, M.; Jensen, P. Ø.; Høiby, N. The in vivo Biofilm. *Trends Microbiol*. **2013**, *21*,466-474.

5. Donlan, R. M.; Costerton, J. W. Biofilms: Survival Mechanisms of Clinically Relevant Microorganisms. *Clin. Microbiol. Rev.* **2002**, *15*, 167–193.

6. Toprak, E.; Veres, A.; Michel, J. B.; Chait, R.; Hartl, D. L.; Kishony, R. Evolutionary Paths to Antibiotic Resistance Under Dynamically Sustained Drug Stress. *Nat. Genet.* **2011**, *44*, 101-105.

7. Hurdle, J. G.; O'Neill, A. J.; Chopra, I.; Lee, R. E. Targeting Bacterial Membrane Function: An Underexploited Mechanism for Targeting Persistent Infections. *Nat. Rev. Microbiol.* **2011**, *62*, 62-75.

8. Silhavy, T. J.; Kahne, D.; Walker, S. The Bacterial Cell Envelope. *Cold Spring Harb. Perspect. Biol.* **2010**, 2, a000414.

9. Papo, N.; Shai, Y. A Molecular Mechanism for Lipopolysaccharide Protection of Gram-Negative Bacteria from Antimicrobial Peptides. *J. Biol. Chem.* **2005**, *280*, 10378-10387.

10. Rosenfeld, Y.; Papo, N.; Shai, Y.; Endotoxin (Lipopolysaccharide) Neutralization by Innate Immunity Host-Defense Peptides. *J. Biol. Chem*. **2006**, *281*, 1636-1643

11. Hamley, I. W. Lipopeptides: From Self-Assembly to Bioactivity. *Chem Commun.* **2015**, *51*, 8574-8583.

12. Hancock, R. E. W.; Diamond, G. The Role of Cationic Antimicrobial Peptides in Innate Host Defences. *Trends Microbiol.* **2000**, *8*, 402–410

13. Stach, M.; Siriwardena, T. N.; Köhler, T.; Delden, C. van Delden; Darbre, T.; Reymond, J. L. Combining Topology and Sequence Design for The Discovery of Potent Antimicrobial Peptide Dendrimers Against Multidrug-Resistant Pseudomonas aeruginosa. *Angew. Chem. Int. Ed.,* **2014**, *53*, 12827-12831.

14. Konai, M. M.; Adhikary, U.; Samaddar, S.; Ghosh, C.; Haldar, J. Structure-Activity Relationship of Amino Acid Tunable Lipidated Norspermidine Conjugates: Disrupting Biofilms with Potent Activity against Bacterial Persisters. *Bioconjug. Chem*. **2015**, *26*, 2442-2453.

15. Liu, D.; Choi, S.; Chen, B.; Doerksen, R. J.; Clements, D. J.; Winkler, J. D.; Klein, M. L.; DeGrado, W. F. Nontoxic Membrane-Active Antimicrobial Arylamide Oligomers. *Angew. Chem. Int. Ed.* **2004**, *43*, 1158-1162.

16. Moon, S. H.; Zhang, X.; Zheng, G.; Meeker, D. G.; Smeltzer, M. S.; Huang, E. Novel Linear Lipopeptide Paenipeptins with Potential for Eradicating Biofilms and Sensitizing Gram-Negative Bacteria to Rifampicin and Clarithromycin. *J. Med. Chem.* **2017**, *60*, 9630–9640.

17. Rončević, T.; Vukičević, D.; Ilić, N.; Krce, L.; Gajski, G.; Tonkić, M.; Goić-Barišić, I.; Zoranić, L.; Sonavane, Y.; Benincasa, M.; Juretić, D.; Maravić, A.; Tossi, A. Antibacterial Activity Affected by The Conformational Flexibility in Glycine-Lysine Based A-Helical Antimicrobial Peptides. *J. Med. Chem.* **2018**, *61*, 2924–2936.

18. Tang, H.; Doerksen, R. J.; Jones, T. V.; Klein, M. L.; Tew, G. N. Biomimetic Facially Amphiphilic Antibacterial Oligomers with Conformationally Stiff Backbones. *Chem. Biol.* **2006**, *13*, 427-435.

19. Uppu, D. S. S. M.; Konai, M. M.; Baul, U.; Singh, P.; Siersma, T. K.; Samaddar, S.; Vemparala, S.; Hamoen, L. W.; Narayana, C.; Haldar, J. Isosteric Substitution in Cationic-Amphiphilic Polymers Reveals An Important Role For Hydrogen Bonding in Bacterial Membrane Interactions. *Chem. Sci.* **2016**, *7*, 4613-4623.

20. Siriwardena, T. N.; Capecchi, A.; Gan, B. H.; Jin, X.; He, R.; Wei, D.; Ma, L.; Köhler, T.; van Delden, C.; Javor, S.; Reymond, J. L. Optimizing Antimicrobial Peptide Dendrimers in Chemical Space. *Angew. Chem. Int. Ed.* **2018**, *57*, 8483-8487.

21. Lai, X. Z.; Feng, Y.; Pollard, J.; Chin, J. N.; Rybak, M. J.; Bucki, R.; Epand, R. F.; Epand, R. M.; Savage, P. B. Ceragenins: Cholic Acid-Based Mimics of Antimicrobial Peptides. *Acc. Chem. Res.* **2008**, *41*, 1233–1240.

22. Ding, B.; Yin, N.; Liu, Y.; Cardenas-Garcia, J.; Evanson, R.; Orsak, T.; Fan, M.; Turin, G.; Savage, P. B. Origins of Cell Selectivity of Cationic Steroid Antibiotics. *J. Am. Chem. Soc.* **2004**, *126*, 13642-13648.

23. Bansal, S.; Singh, M.; Kidwai, S.; Bhargava, P.; Singh, A.; Sreekanth, V.; Singh, R.; Bajaj, A. Bile Acid Amphiphiles with Tunable Head Groups as Highly Selective Antitubsercular Agents. *MedChemComm* **2014**, *5*, 1761-1768.

24. Savage, P. B. Design, Synthesis and Characterization of Cationic Peptide and Steroid Antibiotics. *Eur. J. Org. Chem.* **2002**, *5*, 759-768.

25. Singla, P., Dalal, P., Kaur, M., Arya, G., Nimesh, S., Singh, R., Salunke, D. B. Bile Acid Oligomers and Their Combination with Antibiotics to Combat Bacterial Infections. *J. Med. Chem.* **2018**, *61*, 10265–10275.

26. Wiegand, I.; Hilpert, K.; Hancock, R. E. W. Agar and Broth Dilution Methods to Determine the Minimal Inhibitory Concentration (MIC) of Antimicrobial Substances. *Nat. Protoc*. **2008**, *3*, 163-175.

27. Chan, D. I.; Prenner, E. J.; Vogel, H. J. Tryptophan and Arginine-Rich Antimicrobial Peptides: Structures and Mechanisms of Action. *Biochim. Biophys. Acta-Biomembr.* **2006**, 1758, 1184-1202.

28. Boags, A.; Hsu, P. C.; Samsudin, F.; Bond, P. J., Khalid, S. Progress in Molecular Dynamics Simulations of Gram-Negative Bacterial Cell Envelopes. *J. Phys. Chem. Lett.* **2017**, *8*, 2513-2518.

29. Jefferies, D.; Hsu, P. C.; Khalid, S. Through The Lipopolysaccharide Glass: A Potent Antimicrobial Peptide Induces Phase Changes in Membranes. *Biochemistry* **2017**, *56*, 1672-1679.

30. Castillo, N.; Monticelli, L.; Barnoud, J.; Tieleman, D. P. Free energy of WALP23 dimer association in DMPC, DPPC, and DOPC bilayers. *Chem. Phys. Lipids.* **2013**, *169*, 95-105.

31. Nagpal, S.; Tiwari, S.; Mapa, K.; Thukral, L. Decoding Structural Properties of a Partially Unfolded Protein Substrate: En Route to Chaperone Binding. *PLoS Comput. Biol.* **2015**, *11*, e1004496.

32. Doncheva, N. T.; Klein, K.; Domingues, F. S.; Albrecht, M. Analyzing and Visualizing Residue Networks of Protein Structures. *Trends Biochem. Sci.* **2011**, *36*, 179-182.

33. Singh, M.; Bansal, S.; Kundu, S.; Kidwai, S.; Bhargava, P.; Singh, A.; Motiani, R. K.; Shyam, R.; Sreekanth, V.; Sengupta, S.; Bajaj, A. Synthesis, Structure-Activity Relationship, and Mechanistic Investigation of Lithocholic Acid Amphiphiles for Colon Cancer Therapy. *MedChemComm.* **2015**, *6*, 192-201.

34. Moore, R. A.; Bates, N. C.; Hancock, R. E. W. Interaction of Polycationic Antibiotics with *Pseudomonas Aeruginosa* Lipopolysaccharide and Lipid a Studied by Using Dansyl-Polymyxin. *Antimicrob. Agents Chemother.* **1986**, *29*, 496–500.

35. Uppu, D. S. S. M.; Haldar, J. Lipopolysaccharide Neutralization by Cationic-Amphiphilic Polymers through Pseudoaggregate Formation. *Biomacromolecules.* **2016**, *17*, 862-873.

36. Mozsolits, H.; Wirth, H. J; Werkmeister, J.; Aguilar, M. I. Analysis of Antimicrobial Peptide Interactions with Hybrid Bilayer Membrane Systems Using Surface Plasmon Resonance. *Biochim. Biophys. Acta-Biomembr.* **2001**, *1512*, 64-76.

37. Epand, R. F.; Maloy, W. L.; Ramamoorthy, A. ; Epand, R. M. Probing The "Charge Cluster Mechanism" in Amphipathic Helical Cationic Antimicrobial Peptides. *Biochemistry.* **2010**, *49*, 4076–4084.

38. Loh, B.; Grant C.; Hancock, R. E. Use of the Fluorescent Probe 1-N-Phenylnaphthylamine to Study the Interactions of Aminoglycoside Antibiotics with the Outer Membrane of *Pseudomonas aeruginosa*. *Antimicrob. Agents Chemother*. **1984**, *4*, 546–551.

39. Sims, P. J.; Waggoner, A. S.; Wang, C. H.; Hoffman, J. F. Studies on the Mechanism by Which Cyanine Dyes Measure Membrane Potential in Red Blood Cells and Phosphatidylcholine Vesicles. *Biochemistry*. **1974**, *13*, 3315–3330.

40. Lewis, K. Platforms for Antibiotic Discovery. *Nat. Rev. Drug Discov*. **2013**, *12*, 371-387.

41. Bjarnsholt, T.; Ciofu, O.; Molin, S.; Givskov, M.; Høiby, N. Applying Insights from Biofilm Biology to Drug Development - Can A New Approach be Developed? *Nat. Rev. Drug Discov*., **2013**, *12*, 791-808.

42. Yu, K.; Lo, J. C.Y.; Yan, M.; Yang, X.; Brooks, D. E.; Hancock, R. E.W.; Lange, D.; Kizhakkedathu, J. N. Anti-Adhesive Antimicrobial Peptide Coating Prevents Catheter Associated Infection in A Mouse Urinary Infection Model. *Biomaterials.* **2017**, *116*, 69-81.

43. Fisher, L. E.; Hook, A. L.; Ashraf, W.; Yousef. A.; Barrett, D.A.; Scurr, D. J.; Chen, X.; Smith, E. F.; Fay, M.; Parmenter, C. D. J.; Parkinson, R.; Bayston. R. Biomaterial Modification of Urinary Catheters with Antimicrobials to Give Long-Term Broad Spectrum Antibiofilm Activity. *J. Control Release* **2015**, *202*, 57–64.

44. Uppu, D. S. S. M.; Samaddar, S.; Ghosh, C.; Paramanandham, K.; Shome, B. R.; Haldar, J. Amide Side Chain Amphiphilic Polymers Disrupt Surface Established Bacterial Bio-Films and Protect Mice from Chronic *Acinetobacter baumannii* Infection. *Biomaterials.* **2016**, *74*, 131-143.

Figure Legends

Figure 1. (A) General molecular structure of Cholic Acid Peptide conjugates (CAPs) (**1-20**) where three hydroxyl termini were derivatized with dipeptides of X-G- motif (X = any natural amino acid, G = glycine) and carboxyl terminal is modified with benzyl group. (B) Molecular structures of Valine-Glycine- (CAP **3**), Tryptophan-Glycine- (CAP **10**), Glutamic Acid-Glycine-(CAP **15**), and Lysine-Glycine- (CAP **18**) derived CAPs.

Figure 2. (A) Representative snapshot of MD simulations-derived structures in the presence of model LPS membranes and different CAPs at 500 ns. (B) Membrane thickness is plotted as a function of X-Y dimension of simulation box (top view) to quantify geometric differences. The color bar indicated the thickness values with blue (lower) values towards the spectrum shows membrane thinning.

Figure 3. (A) Mapping of root mean square fluctuation (RMSF) as a function of each atom in CAPs **3**, **10**,**15** and **18**. (B) Superimposed conformations of four CAPs across different time points in grey and representative coloured line conformation shows the top cluster in each trajectory.

Figure 4. Global intra-molecular network for CAPs at 0 and 500 ns showing the CA backbone and number of edges formed by each CAP at 0 and 500 ns. The circles/edges/atom numbers are coloured in orange with different intensities (low to high), with dark orange nodes connected to multiple atoms.

Figure 5. (A) Change in anisotropy of Diphenylhexatriene (DPH) confirm the ability of CAP **3** to disrupt the membranes more effectively than other CAPs. DPH-doped model Gram-negative bacterial membranes were incubated with CAPs and change in anisotropy was measured by fluorescence. Data is presented as Mean ± SD of three replicates and statistical analysis was performed by unpaired two-tailed Student's *t*-test. (B) LPS binding abilities of CAPs show strongest binding of CAP **3** over other CAPs. Dansyl Polymyxin B-LPS complexes were incubated with different CAPs and change in fluorescence of Dansyl-Polymyxin was measured. Data is presented as Mean ± SD of three replicates and statistical analysis was performed by unpaired two-tailed Student's *t*-test. (C) Change in fluorescence of BODIPY show the strong interactions of CAP **3** with LPS causing its disintegration. BODIPY-LPS aggregates were incubated with different CAPs and change in fluorescence was measured. Data is presented as Mean ± SD of three replicates and statistical analysis was performed by unpaired two-tailed Student's *t*-test. (D-F) Surface Plasmon Resonance based sensorgrams of CAPs **3** (D), **15** (E) and **18** (F) confirm irreversible and strong binding of CAP **3** over other CAPs. (G) Binding constants calculated from sensorgrams of **3**, **15** and **18** after binding with bacterial membranes show strong association of CAP **3**. Data is presented as an average of three replicates.

Figure 6. (A) Change in fluorescence of *N*-phenyl naphthylamine (NPN) show enhanced ability of CAP **3** to perturb the outer bacterial membranes as compared to other CAPs. NPN stained *E. coli* were incubated with different CAPs (8 μM) and change in fluorescence intensity was measured with time. Data is presented as an average of three replicates. (B) Time dependent change in $DISC_2(5)$ fluorescence in *E. coli* show better ability of CAP **3** to permeabilize the inner bacterial membranes over other CAPs. $DISC_2(5)$-labelled *E. coli* were treated with different CAPs (8 μM) and change in fluorescence intensity was measured with

time. Data is presented as an average of three replicates. (C) Percentage of Propidium iodide (PI) positive *E. coli* cells show maximum number of dead cells on CAP **3** treatment. *E. coli* were treated with different CAPs at 32 μM, stained with PI and analyzed by flow cytometry. Data is presented as Mean ± SD of four replicates and statistical analysis was performed by unpaired two-tailed Student's *t*-test. (D) Time kill assay confirm the bactericidal effect of CAP **3** on *E. coli* as no colonies observed on treatment. *E. coli* was treated with 1X and 4X MIC_{99} of CAP **3** and CFU analysis was performed at different time points. Data is presented as Mean ± SD of four replicates and statistical analysis was performed using two-way ANOVA. (E) Transmission electron micrographs of untreated and CAP **3** (8 μM) treated *E. coli* at different time show membrane disruption in bacteria on CAP **3** treatment. (F) Fold change in MIC_{99} of CAP **3** and neomycin on pre-treated *E. coli* show inability of the bacteria to develop drug resistance. MIC_{99} of CAP **3** and neomycin was measured on pre-treated samples using broth-dilution assay in four replicates. (G) Bactericidal effect of CAP **3** and ampicillin treatment on persistent and stationary bacteria. Data is presented as Mean ± SD of two replicates and statistical analysis was performed by unpaired two-tailed Student's *t*-test. (H) Fold change in MIC_{99} of CAP **3** and Polymyxin at different CFUs show only 2-fold increase in MIC_{99} of CAP **3** at 10^{12} CFU/mL. MIC_{99} of CAP **3** and Polymyxin was measured at different CFUs using broth-dilution assay in four replicates.

Figure 7. (A-B) Dose-dependent effect of CAP **3** on colony forming units (A) and biofilm biomass (B) of *E. coli* biofilms confirm bactericidal effect of CAP **3**. Pre-formed biofilms were treated with different doses of CAP **3** followed by CFU and biomass quantification using crystal violet. Data is presented as Mean ± SD of three replicates and statistical analysis was performed by unpaired two-tailed Student's *t*-test. (C) Representative fluorescence micrographs of untreated and CAP **3**-treated *E. coli* biofilms confirm bactericidal nature of

CAP **3** with dead bacteria shown in red stained by PI and live bacteria shown in green stained by SYTO9. (D) Quantification of thickness of untreated and CAP **3**-treated biofilms shows significant reduction in thickness on CAP **3** treatment. Data is presented as Mean ± SD of three replicates and statistical analysis was performed by unpaired two-tailed Student's *t*-test. (E) Representative scanning electron micrographs of untreated and CAP **3** treated *E. coli* biofilms show disintegration of the biofilm structure on CAP **3** treatment.

Figure 8. (A) CFU analysis showing the ability of CAP **3**-coated catheters to prevent *E. coli* biofilm formation during *in vitro* conditions. Untreated, DCM- and CAP **3-**coated catheters were incubated with bacteria for three days, and bacterial load on catheters was calculated by CFU analysis. Data is presented as Mean ± SD of three replicates and statistical analysis was performed by unpaired two-tailed Student's *t*-test. # no colonies were observed. (B) CFU analysis showing the effect of CAP **3**-coated catheters in BALB/c mice to prevent biofilm formation by *E. coli*. Untreated, DCM and CAP **3-**coated catheters were implanted in BALB/c mice (n = 3/group) followed by *E. coli* infection, and CFU analysis was performed after three days. Data is presented as Mean ± SD of three mice and statistical analysis was performed by unpaired two-tailed Student's *t*-test. # no colonies were observed. (C) Effect of CAP **3** in reducing the bacterial burden on wounds in BALB/c mice. *E. coli* infected wounds were treated with Ampicillin, CAP **3** and Neomycin for four days and bacterial load was quantified by CFU analysis. Data is presented as Mean ± SD of three mice and statistical analysis was performed by unpaired two-tailed Student's *t*-test. # no colonies were observed. (D) Bioluminescence images showing significant reduction in bioluminescence of Xen 14 *E. coli* wound infections on CAP **3** treatment. Xen 14 *E. coli* infected wounds were treated with CAP **3** for four days and bioluminescence imaging was performed. (E)

Antibacterial activities of CAP **3** against different clinical strains of *E. coli*, *K. pneumoniae, A. baumannii* and its comparison with standard antibiotics. # no colonies were observed.

Figure 1

A

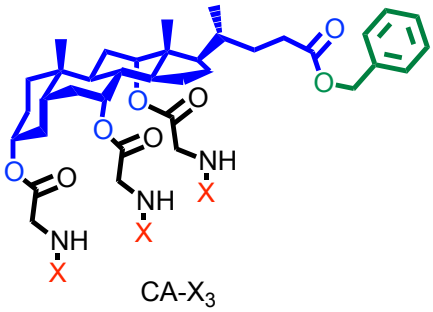

CA-X_3

X = any natural amino acid

1: X = G **6**: X = P **11**: X = S **16**: X = R
2: X = A **7**: X = M **12**: X = T **17**: X = C
3: X = V **8**: X = F **13**: X = H **18**: X = K
4: X = I **9**: X = Y **14**: X = D **19**: X = N
5: X = L **10**: X = W **15**: X = E **20**: X = Q

Cholic Acid Peptide Conjugates (CAPs) (**1**-**20**)

B

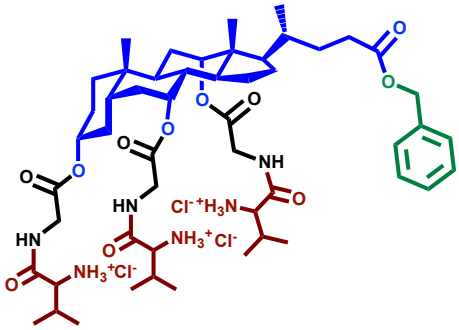

CAP **3**

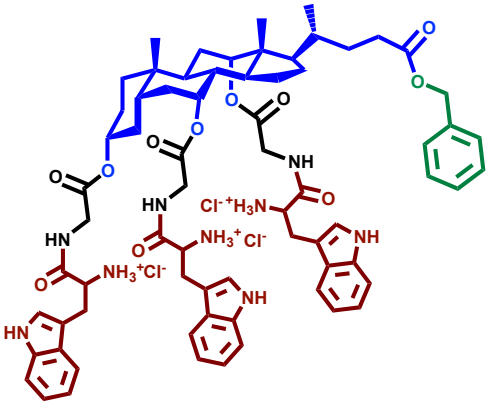

CAP **10**

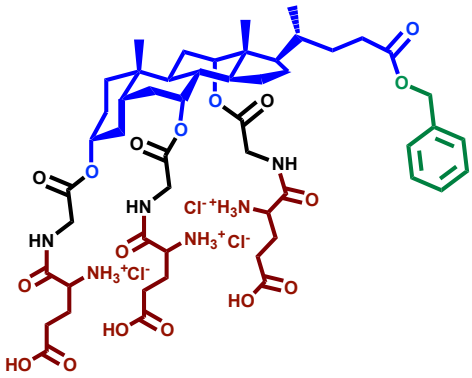

CAP **15**

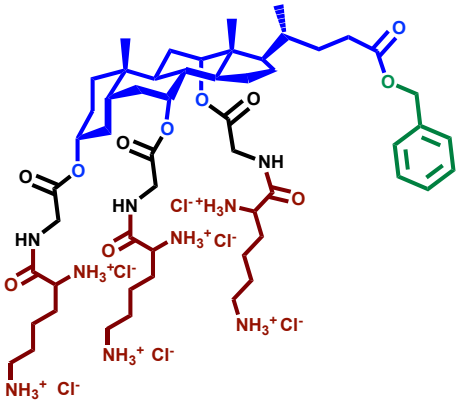

CAP **18**

Figure 2

A B

CAP **3**

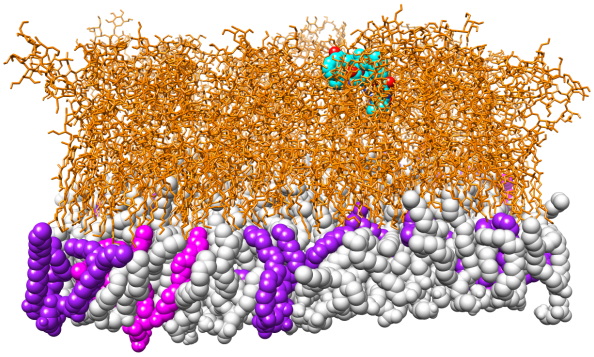

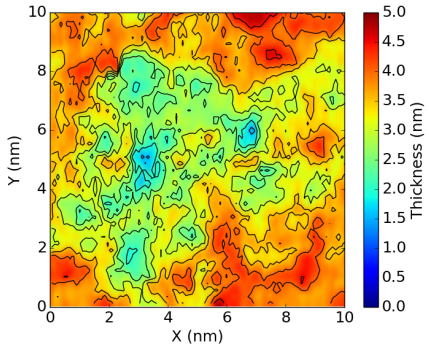

CAP **10**

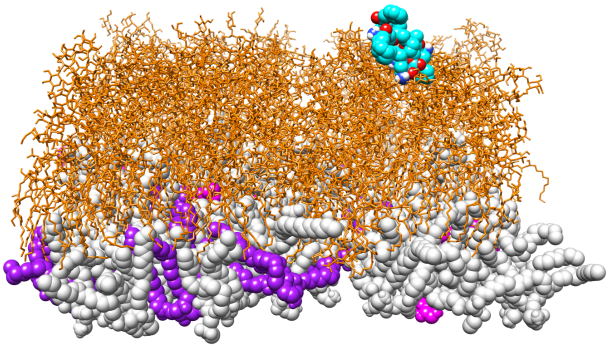

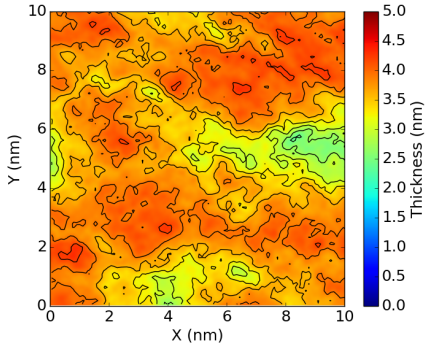

CAP **15**

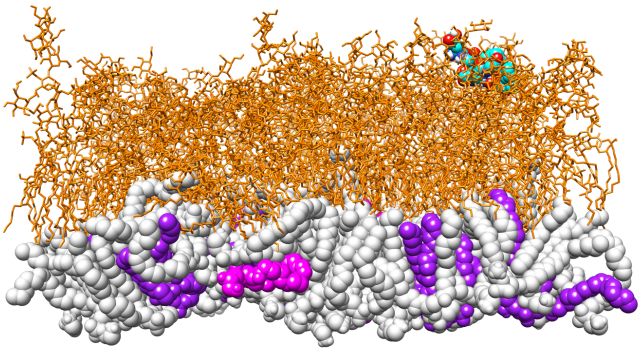

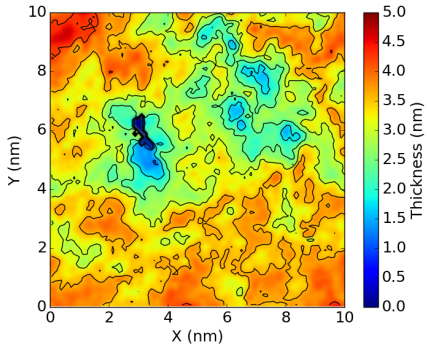

CAP **18**

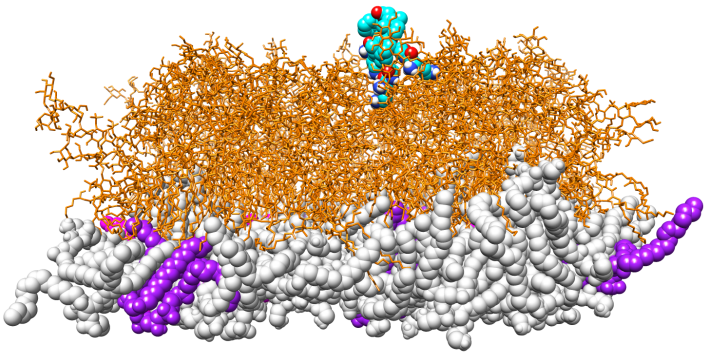

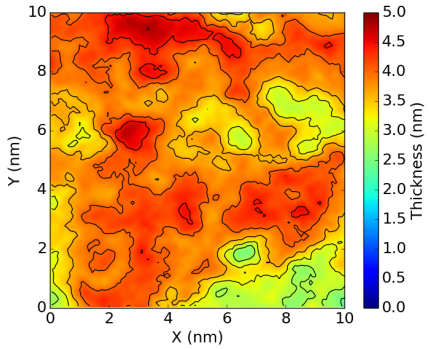

Figure 3

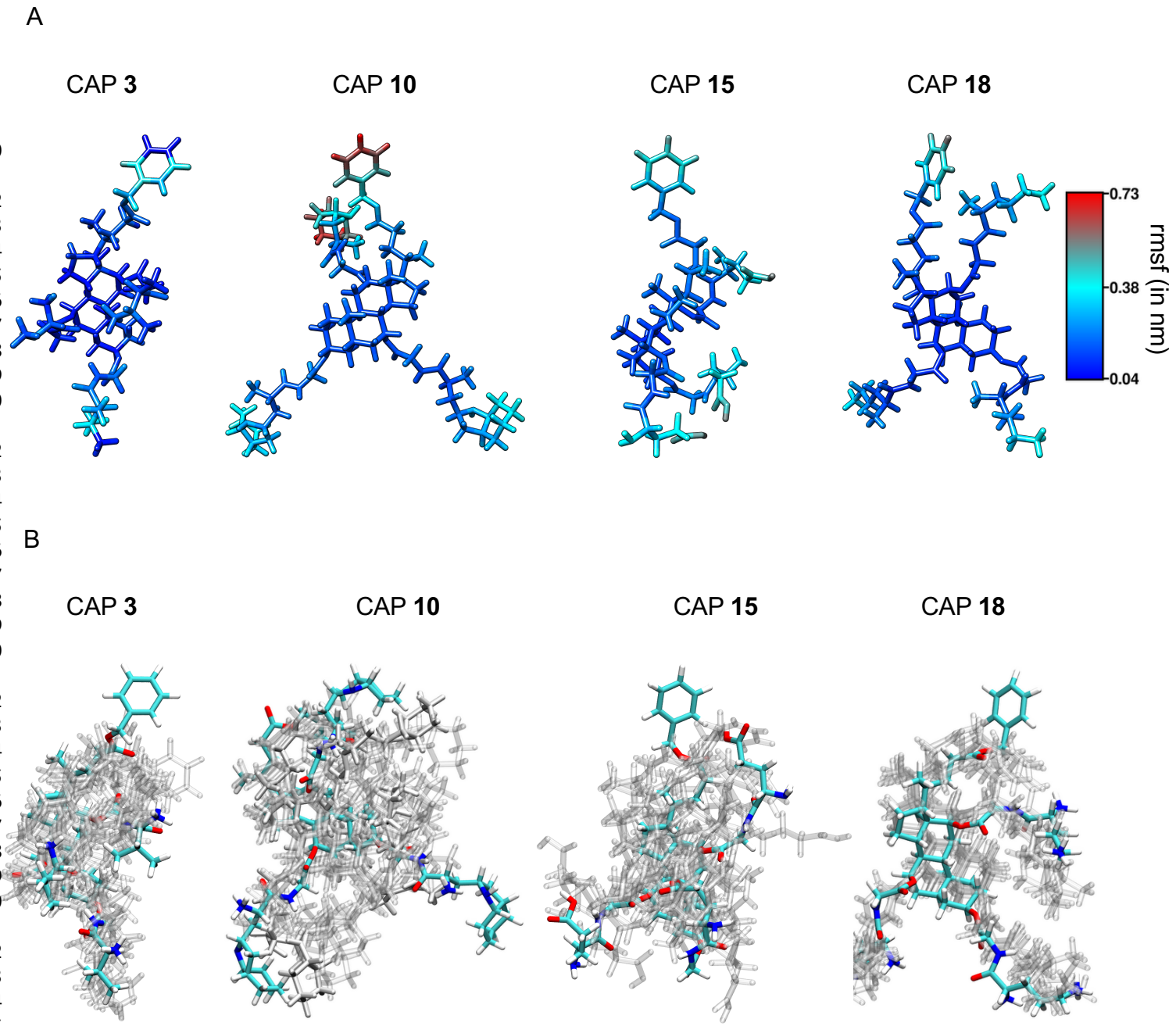
A
CAP 3
CAP 10
CAP 15
CAP 18
0.73
0.38
0.04
rmsf (in nm)
B
CAP 3
CAP 10
CAP 15
CAP 18

Figure 4

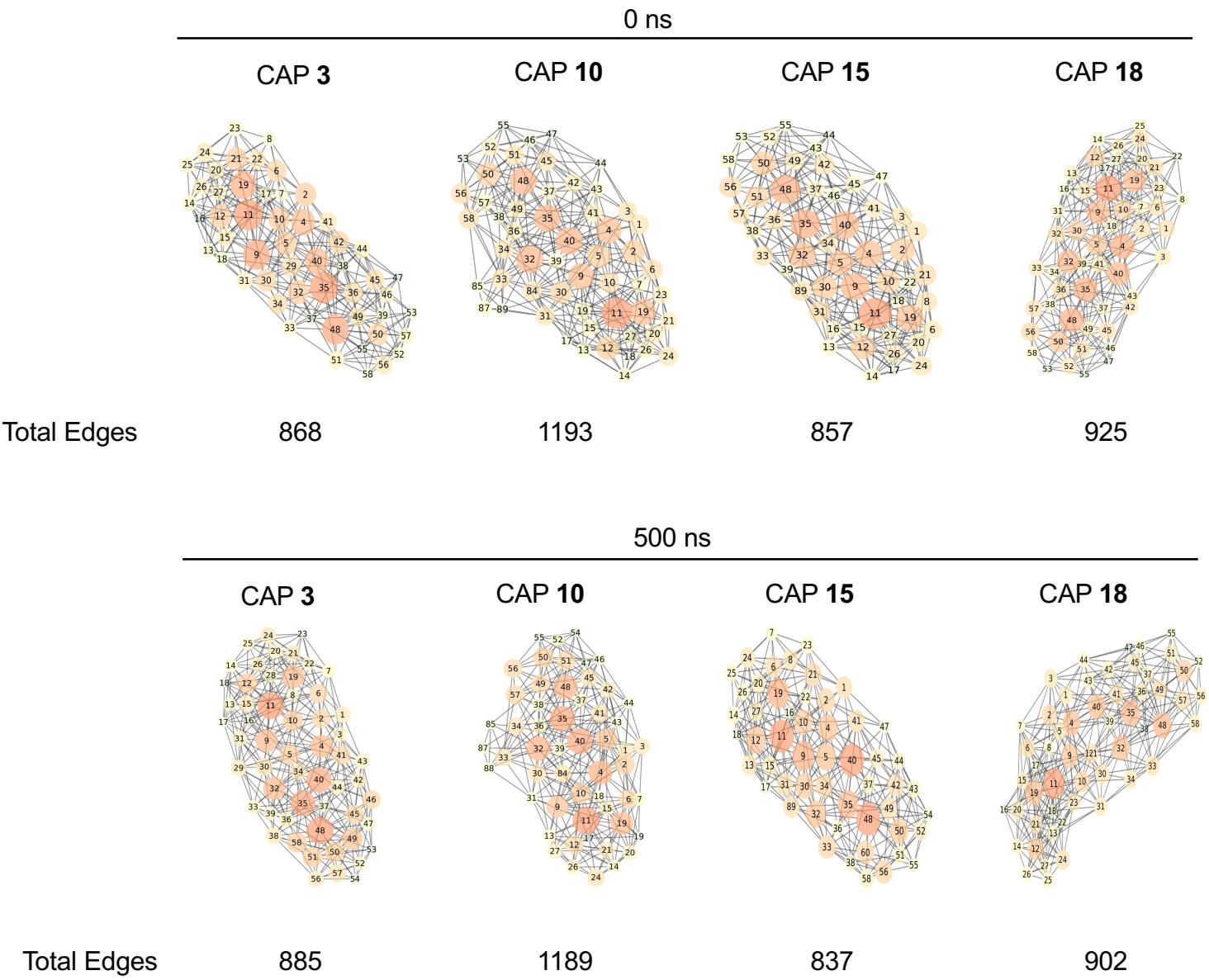
0 ns
CAP 3
CAP 10
CAP 15
CAP 18
Total Edges
868
1193
857
925
500 ns
CAP 3
CAP 10
CAP 15
CAP 18
Total Edges
885
1189
837
902

Figure 5

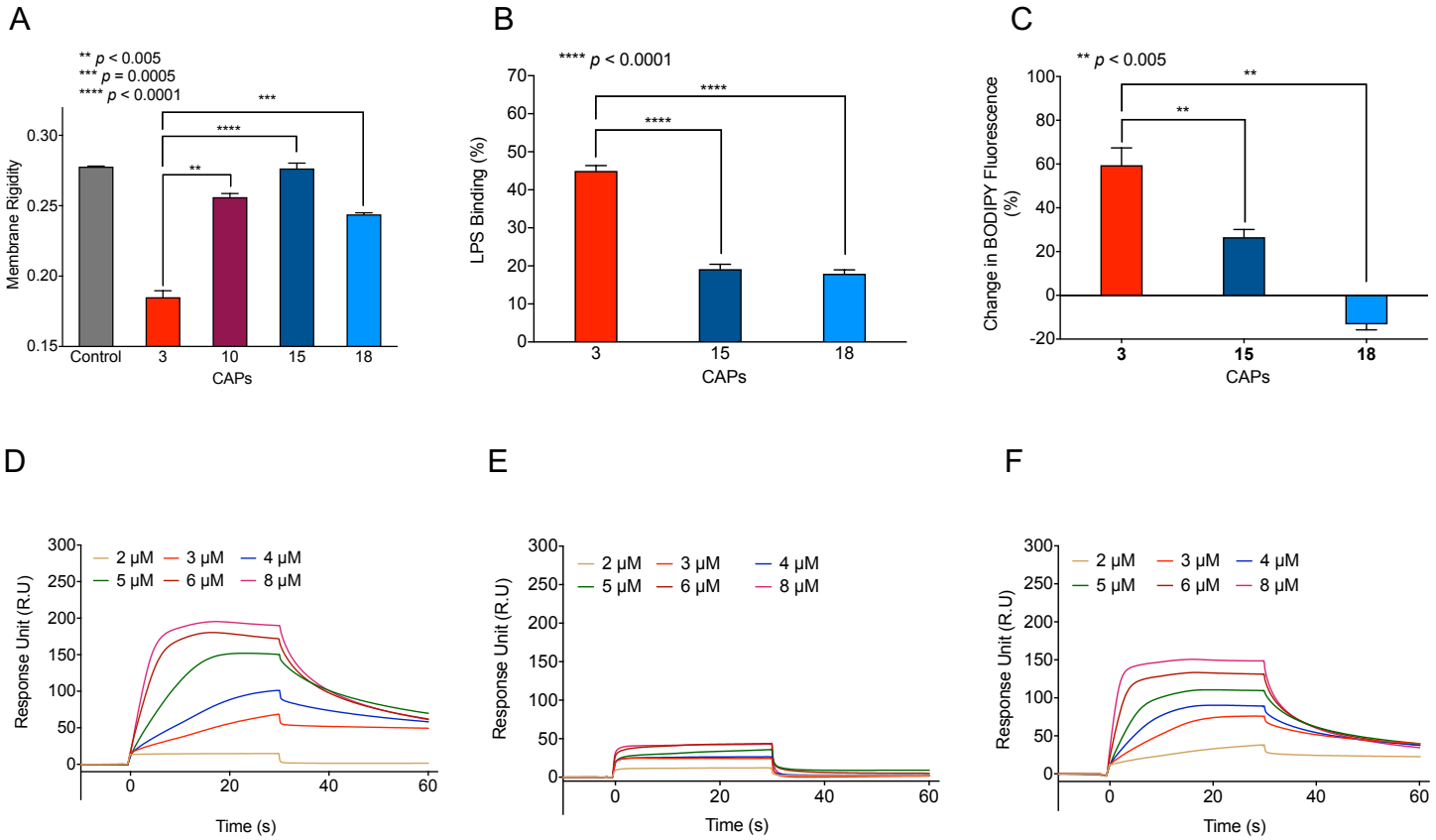

G

CAP	k_{a1}(1/Ms)	k_{d1}(1/s)	K_1(M^{-1})	k_{a2} (1/Ms)	k_{d2} (1/s)	K_2(M^{-1})	K_A (M^{-1})
3	(2.41±0.33)E+4	(6.00±0.85)E-2	4.06E+5	(9.82±1.0) E-3	(4.19±0.58) E-5	2.39E+2	9.60E+07
15	(2.77±0.89)E+4	(9.42±0.97)E-1	3.00E+4	(2.88±0.53) E-2	(5.83±0.12) E-3	4.92	1.71E+05
18	(1.41±0.41)E+5	(2.80±0.89)E-1	5.08E+5	(4.15±0.18) E-2	(3.81±0.61) E-2	1.11	1.07E+06

Figure 6

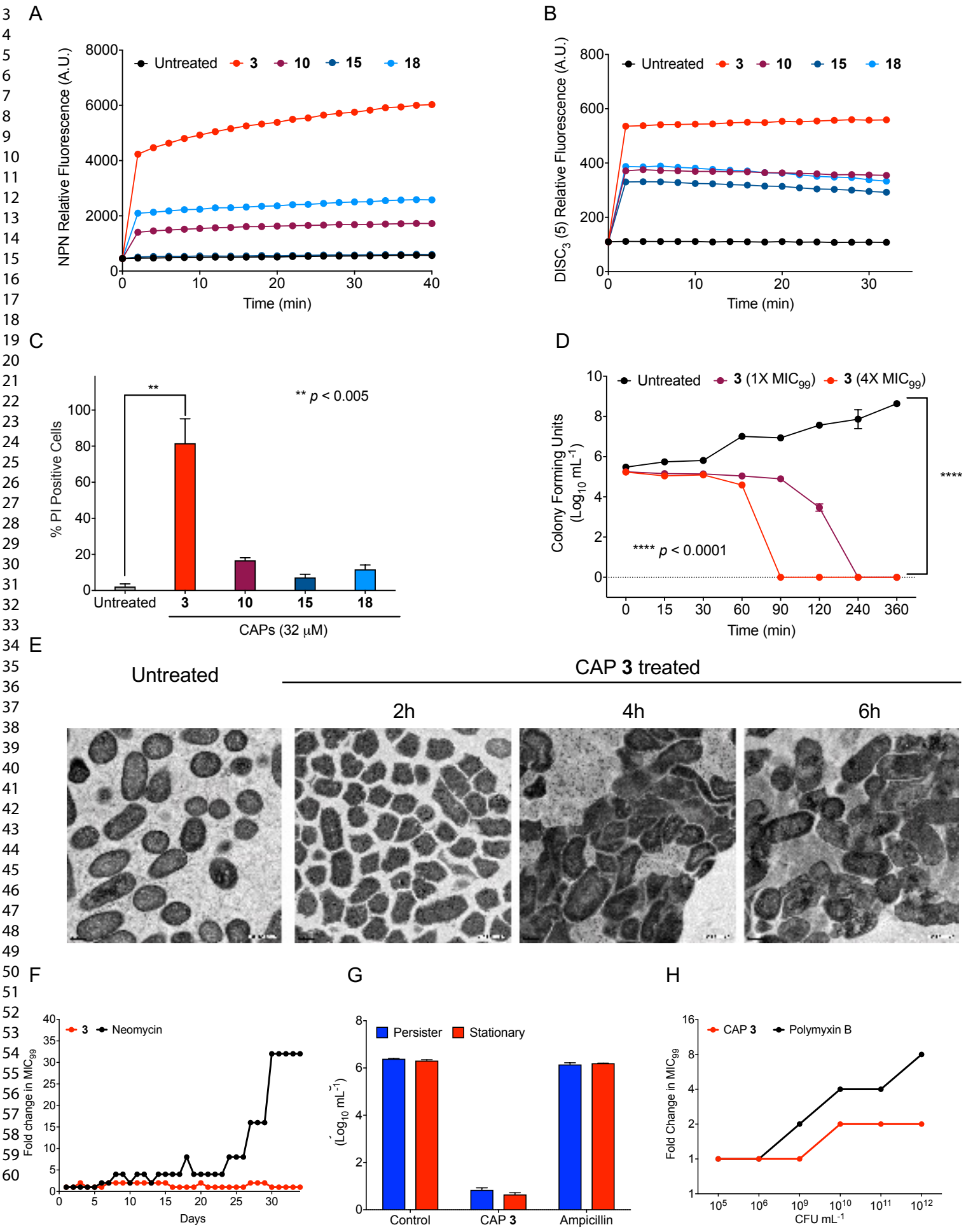
A
NPN Relative Fluorescence (A.U.)
Untreated
3
10
15
18
Time (min)
B
DISC3 (5) Relative Fluorescence (A.U.)
Time (min)
C
% PI Positive Cells
** p < 0.005
Untreated
CAPs (32 μM)
D
Colony Forming Units (Log10 mL-1)
Untreated
3 (1X MIC99)
3 (4X MIC99)
**** p < 0.0001
****
Time (min)
E
Untreated
CAP 3 treated
2h
4h
6h
F
Fold change in MIC99
3
Neomycin
Days
G
Persister
Stationary
(Log10 mL-1)
Control
CAP 3
Ampicillin
H
Fold Change in MIC99
CAP 3
Polymyxin B
CFU mL-1

Figure 7

A

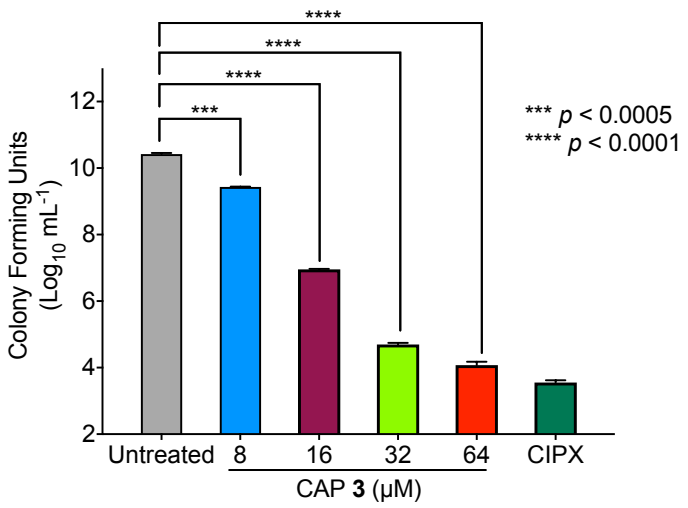

B

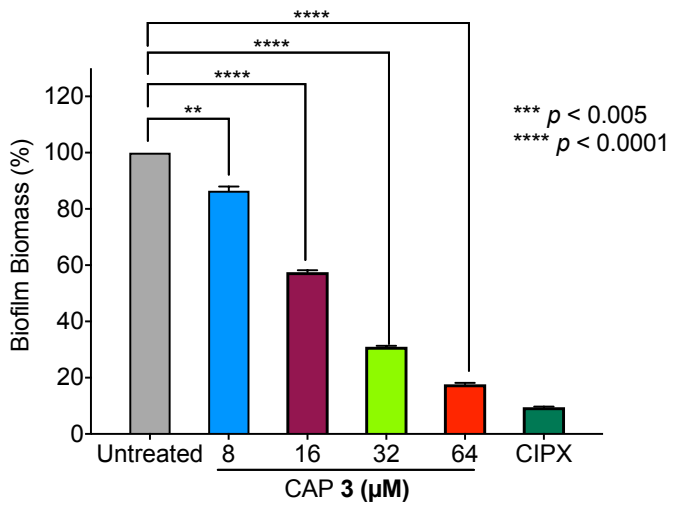

C

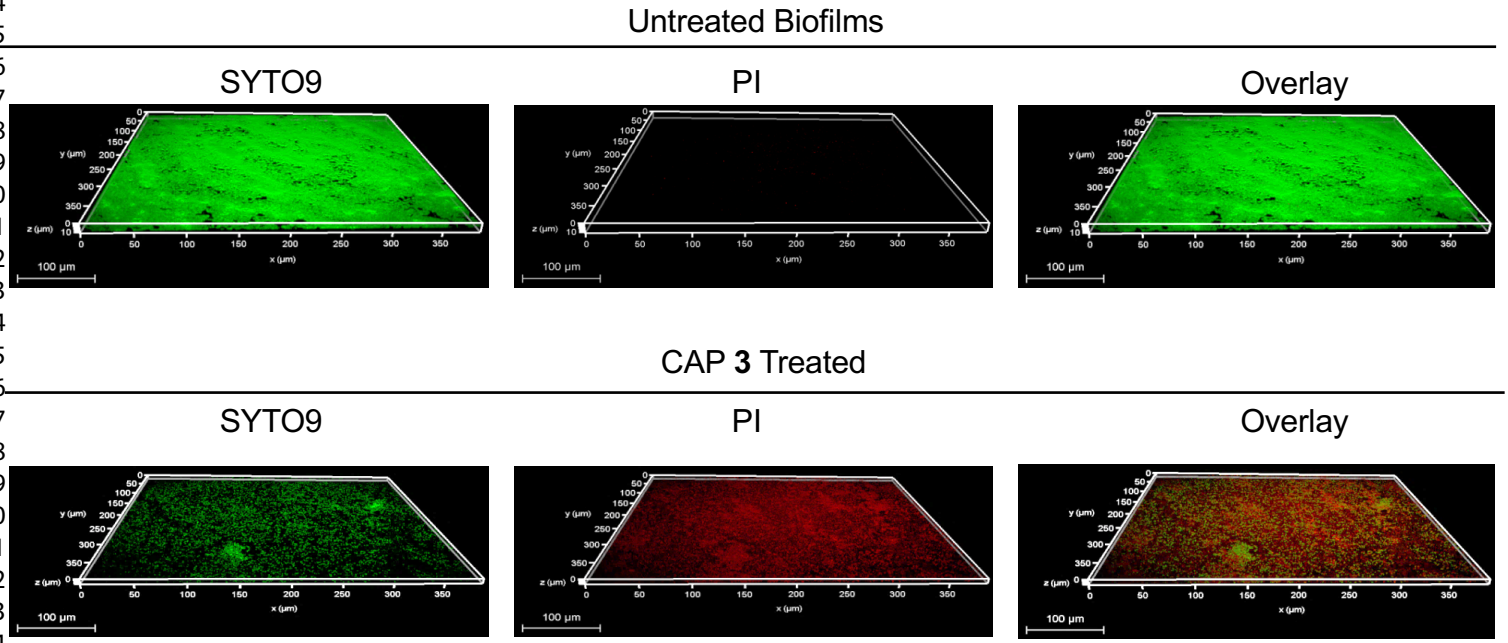

D

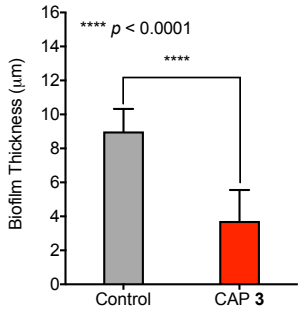

E

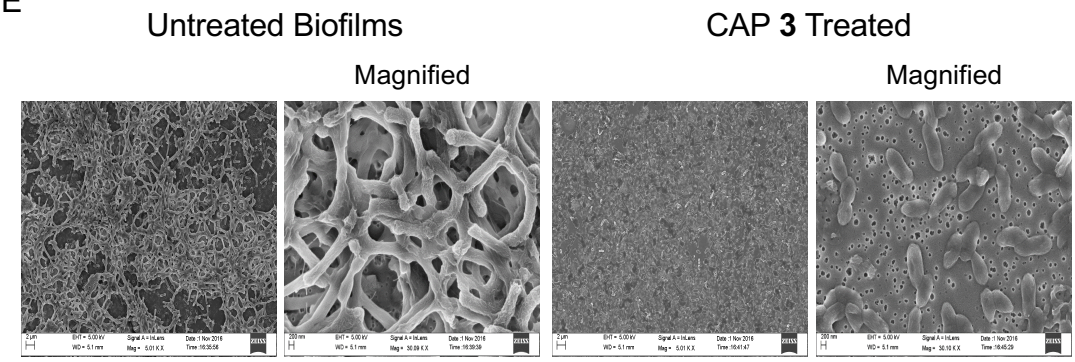

Figure 8

A

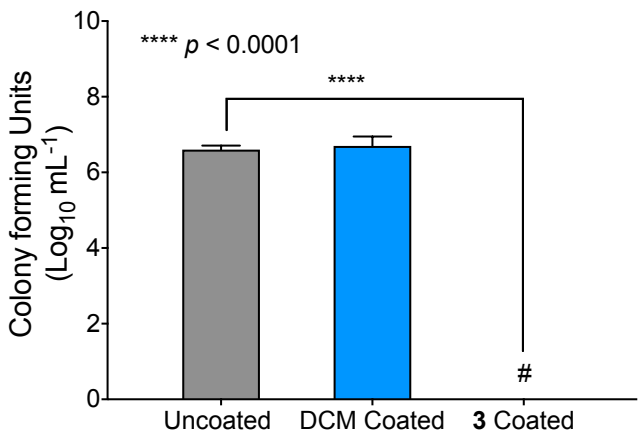

B

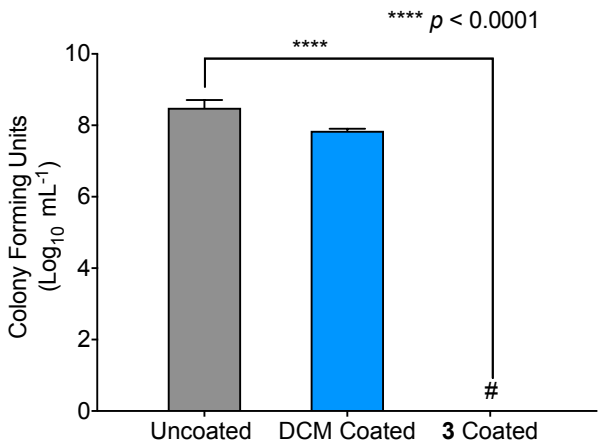

C

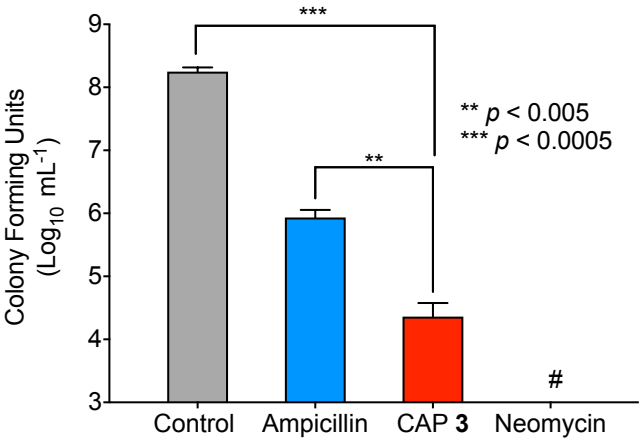

D

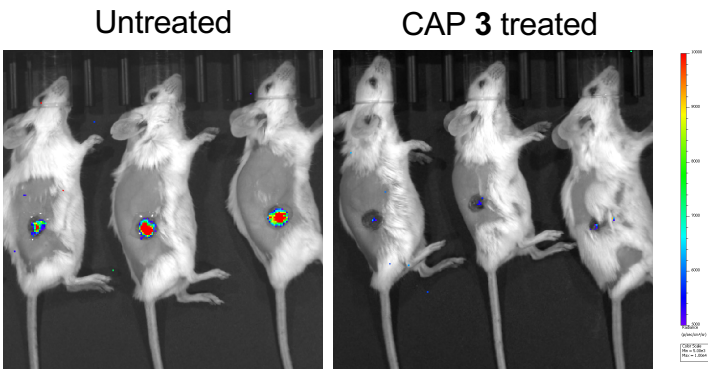

E

	E. coli					*A. baumannii*					*K. pneumoniae*				
	9/44	9/203	6/23	6/27	6/38	4/307	1/303	5/321	4/202	5/412	8/407	8/307	7/47	12823	12744
Amikacin	R	S	R	R	R	R	R	R	R	R	R	R	R	R	R
Ceftazidime	R	R	R	R	R	R	R	R	R	R	R	R	R	R	R
Ciprofloxacin	R	S	R	R	R	R	R	R	R	R	R	R	R	R	R
Meropenem	S	S	S	I	S	R	R	R	R	R	R	R	R	R	S
Imipenem	I	S	S	R	I	R	R	R	R	R	R	R	I	R	I
Piperacillin tazobactum	R	S	R	R	R	R	R	R	R	R	R	R	I	R	R
CAP **3**	8	8	8	4	4	16	16	4	8	4	8	8	4	8	8

Table of Contents Graphic

Cholic Acid-Peptide Conjugate

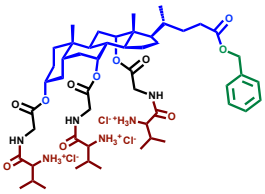

Intramolecular Networking

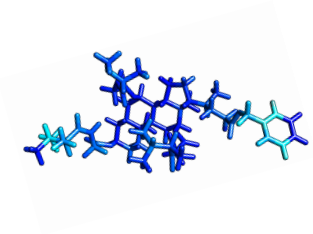

Antimicrobial Action